Mechanism of Al_2CuLi (T_1) Nucleation and Growth

W.A. CASSADA, G.J. SHIFLET, and E.A. STARKE, Jr.

Conventional strain contrast transmission electron microscopy (CTEM) and high-resolution transmission electron microscopy (HRTEM) were performed to establish the nucleation and growth mechanism of Al_2CuLi (T_1) precipitates in an Al-Li-Cu alloy. It is shown that the growth mechanism of T_1 precipitate plates occurs by the diffusional glide of growth ledges composed of $\mathbf{b} = 1/6\langle 112\rangle$ partial dislocations on {111} matrix planes and that the growth ledges migrate by the ledge-kink mechanism, as previously suggested by Cassada *et al.*[1] for this system. T_1 plate nucleation is modeled as the dissociation of a perfect $\mathbf{b} = 1/2\langle 110\rangle$ matrix dislocation in the vicinity of a dislocation jog. The coordinated dissociation of the dislocation line segments on each side of the sessile jog provides the displacement necessary for the formation of a new hexagonal plate or plate ledge. Strain contrast analysis of the Burgers vector of plate edges and the edges of growth ledges indicates the stacking of partial dislocations is of mixed displacement.

I. INTRODUCTION

THE heterogeneous precipitation of T_1 plates on dislocations in Al-Li-Cu alloys is an example of a relatively simple diffusional transformation. Such transformations are common in aluminum alloys, and examples can be found in Al-Ag,[2–6] Al-Li-Cu,[7,8,9] and Al-Mg-Zn.[10] Precipitation in these systems has been referred to as stacking fault precipitation, because the resulting thin plates of the hexagonal phase are postulated to nucleate on stacking faults on {111} planes by dissociation of perfect $\mathbf{b} = 1/2\langle 110\rangle$ dislocations into $\mathbf{b} = 1/6\langle 112\rangle$ partial dislocations. The precipitate plates appear in conventional transmission electron microscopy (CTEM) images as faulted regions bound by partials, where the basal hexagonal precipitate planes are parallel to the {111} matrix planes.

The role of matrix dislocations in the face-centered cubic → hexagonal close-packed (fcc→hcp) transformation was first demonstrated by Nicholson and Nutting[2] for the precipitation of γ' plates in the Al-Ag system. Hren and Thomas[3] used hot-stage TEM to study γ' precipitation in Al-20 Ag and concluded that γ' nucleation is heterogeneous, occurring by the dissociation of matrix dislocations and silver enrichment of the resulting fcc stacking fault *via* Suzuki interaction. This view of hcp nucleation has been used to explain the nucleation of similar phases in other aluminum systems.[9,11–13] More recently, γ' plate growth has been studied in detail with both CTEM and high-resolution TEM (HRTEM) by Howe *et al.*[4,5,6] In their work, the dissociation of matrix dislocations into partials was found not only important to the formation of new plates but also to the formation of new growth ledges, which both lengthen and thicken the γ' plates. Similar studies in the Al-Li-Cu system have produced essentially identical results for T_1 plate growth.[1]

A significant finding from these studies has been to show that the plate edges and the edges of growth ledges on plates, in fact, consist of stacked arrays of partial dislocations. The number of partials comprising the ledge edge will depend on the total ledge height, and the displacement (that is, Burgers vector) associated with each partial may be the same or different. Therefore, the displacement associated with the edge of a growth ledge is the vector sum of its constituent partials.[1,4,6] Volume strain energy minimization produced by the transformation can be considered as the driving force coupling partials of different Burgers vectors at the edges of growth ledges.[14] An important consequence of these findings is that the plate nucleation mechanism cannot be explained in terms of nucleation on fcc stacking faults. Simple dissociation of a dislocation into Shockley partials bounding a stacking fault cannot produce growth ledges comprised of stacked partial dislocation arrays.

An obstacle to a full atomic description of the growth of T_1 plates has resulted from uncertainties in defining its crystal structure.[8,16–21] Hardy and Silcock[7] gave the first description of the hexagonal cell and, noting the absence of glide planes or screw axes in rotation X-ray photographs, concluded that the space group was either P622, P6mm, P6m2, or P6/mmm. Aside from defining the cell parameter ($a = 0.497$ nm, $c = 0.934$ nm) and the four possible space groups, Hardy and Silcock were unable to predict the atomic arrangement from Debye-Scherrer X-ray intensity data.

Huang and Ardell[15] attempted to fit the X-ray intensity data of Hardy and Silcock[7] by calculating X-ray intensities for various structural models of T_1. Using this approach, Huang and Ardell were able to propose a crystal structure for T_1 that gave good agreement with experimental electron diffraction patterns obtained in several low-order matrix orientations. The Huang and Ardell structure possesses the same cell parameters determined by Hardy and Silcock and belongs to the P6/mmm space group. Stacking within the cell consists of three compositionally distinct layers in the order ABCB . . ., where A and C are ordered close-packed arrangements of Al and Li atoms in rations of 1:2 and 2:1, respectively, and the B layers are random non-close-packed arrangements of Al and Cu atoms in the ratio of 1:1.

W.A. CASSADA, formerly Graduate Student, Department of Materials Science, University of Virginia, is Research Scientist, Reynolds Metals Company, Richmond, VA 23219. G.J. SHIFLET, Professor, Department of Materials Science, and E.A. STARKE, Jr., Earnest J. Oglesbee Professor and Dean, School of Engineering and Applied Science, are with with University of Virginia, Charlottesville, VA 22903.

Manuscript submitted December 18, 1989.

Point and space group analysis performed on bulk T_1 crystals of stoichiometric composition (Al_2CuLi) using convergent beam electron diffraction (CBED) was attempted by Cassada *et al.*,[18] but their Al_2CuLi samples contained a high density of stacking faults which prevented symmetry analysis. Vecchio and Williams,[19] however, used CBED to conclude that the T_1 space group is P6/mmm, and that their results agreed well with the proposed cell of Huang and Ardell.[15]

Three separate groups have investigated the structure of T_1 using HRTEM.[1,20,21] By treating the B compositional layer as close-packed, Cassada *et al.*[1] employed a modified version of the Huang and Ardell T_1 structure as the basis for interpretation of HRTEM images. This arrangement maintains the sequence of compositional layers (ABCB . . .) but treats the stacking of T_1 layers as ABAB . . ., that is, the stacking of close-packed planes. A close-packed structure allowed Cassada *et al.* to describe the nucleation and growth of T_1 in terms of the migration of coupled pairs of partial dislocations. Similarly, Radmilovich and Thomas[21] assumed a close-packed modification of the Huang and Ardell structure in the interpretation of HRTEM images.

Perceiving problems with the Huang and Ardell T_1 structure,[15] Howe *et al.*[20] employed image simulation of HRTEM images to suggest a different T_1 structure. In this model of T_1, a four-layer cell is proposed which consists of stacking of A_1BA_2C layers, where all the layers are close-packed. The B and C layers are compositionally different, A_1 is mostly Al, and A_2 is mostly Li. This cell produces the best agreement to date with experimental electron diffraction patterns and HRTEM images but departs from P6/mmm space group symmetry. Despite different views of the T_1 structure, the description of the nucleation and growth of T_1 plates as proposed by Cassada *et al.*[1] is valid for either structure.

In this paper, T_1 plate nucleation on matrix dislocations is examined with CTEM and HRTEM to better understand the role of matrix dislocations as nucleation sites and their effect on T_1 plate growth. An alternative to the view of nucleation on stacking faults is proposed based on our observations. This alternative mechanism will be extended to explain the formation of growth (plate thickening) ledges on existing plates from acquisition of matrix dislocations. Such a fundamental understanding of T_1 plate nucleation and growth will also allow a better understanding of the effect of plastic strain prior to artificial aging on the resultant T_1 distribution.

II. EXPERIMENTAL PROCEDURE

The Al-2.45Li-2.45Cu-0.18Zr alloy used in this work was prepared by the Reynolds Metals Company as 0.012-m rolled plate. Samples were solution heat-treated at 823 K (550 °C) for 30 minutes and cold-water quenched. Isothermal aging at 463 K (190 °C) was done in an oil bath for times ranging between 3 and 550 hours.

Thin TEM foils were produced by electropolishing the disk in a twin-jet apparatus at 13 V direct current (DC). A 3:1 methanol:nitric acid solution cooled to −20 °C was used as the electrolyte. A PHILLIPS 400T was used for CTEM, while HREM imaging was done at the National Center for Electron Microscopy (Berkeley, CA) on the JEOL ARM1000 operating at 600 KeV with an undersaturated LaB_6 filament. Through focus image series for HREM were taken in $\langle 10\bar{1}0\rangle_{T_1} /\!/ \langle 110\rangle_\alpha$ and $\langle 1\bar{2}10\rangle_{T_1} /\!/ \langle \bar{1}\bar{1}2\rangle_\alpha$ zone axes using a 6.5-nm^{-1}-radius objective aperature.

III. RESULTS AND DISCUSSION

A. *Introduction*

Several important features of the T_1 precipitate plates can be observed in the overaged microstructure (72 hours, 190 °C). Figures 1 through 4 are CTEM images of a single region in various beam orientations, where the individual intersection points of T_1 plates are labeled A through E in each micrograph. Two types of intersections are generally observed for T_1 plates: complete penetration of one plate variant through another (intersection points A, B, and C) or impingement of one plate variant upon another (intersection points D and E).

The two T_1 variants of interest appear as thin lines in Figure 1, where $\mathbf{B} = [110]_{Al}$. In this orientation, the corresponding habit planes $(\bar{1}11)$ and $(1\bar{1}1)$ are parallel to the beam direction, resulting in the narrowest image width for the plates on these matrix planes. The broad T_1 images marked in Figure 1 coincide with plates whose habits lie on $(11\bar{1})$ and (111) matrix planes which are equally inclined with respect to the beam direction (35.3 deg). The corresponding $\mathbf{B} = [110]_{Al}$ selected area diffraction (SAD) pattern is shown in Figure 1 (inset), where the

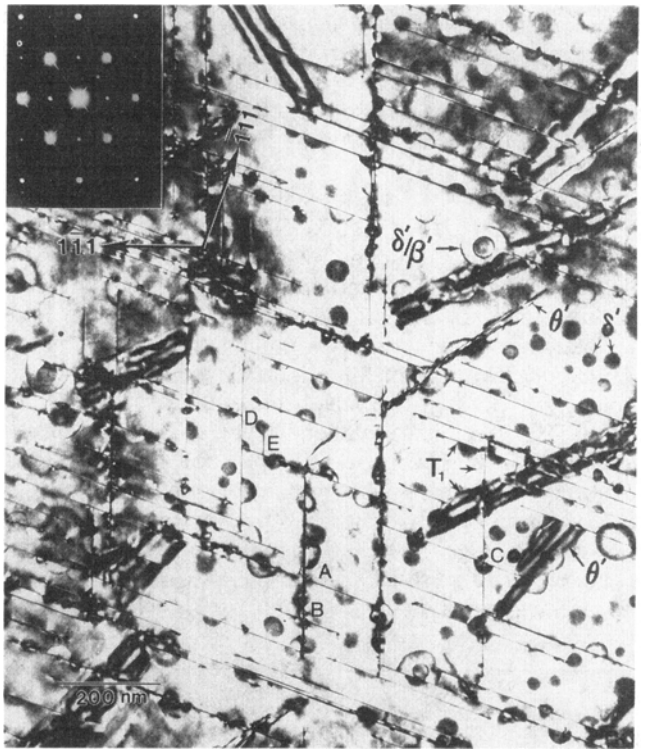

Fig. 1—**B** = [110] orientation for material aged 72 h at 190 °C showing various phases in the microstructure. T_1 variants on $(\bar{1}11)$, $(1\bar{1}1)$, and $(11\bar{1})$ are marked. Inset: SAD pattern, **B** = [110], indicating the presence of T_1 plates on three (111) variants. $\mathbf{B} = [\bar{1}2\bar{1}3]_{T_1}$.

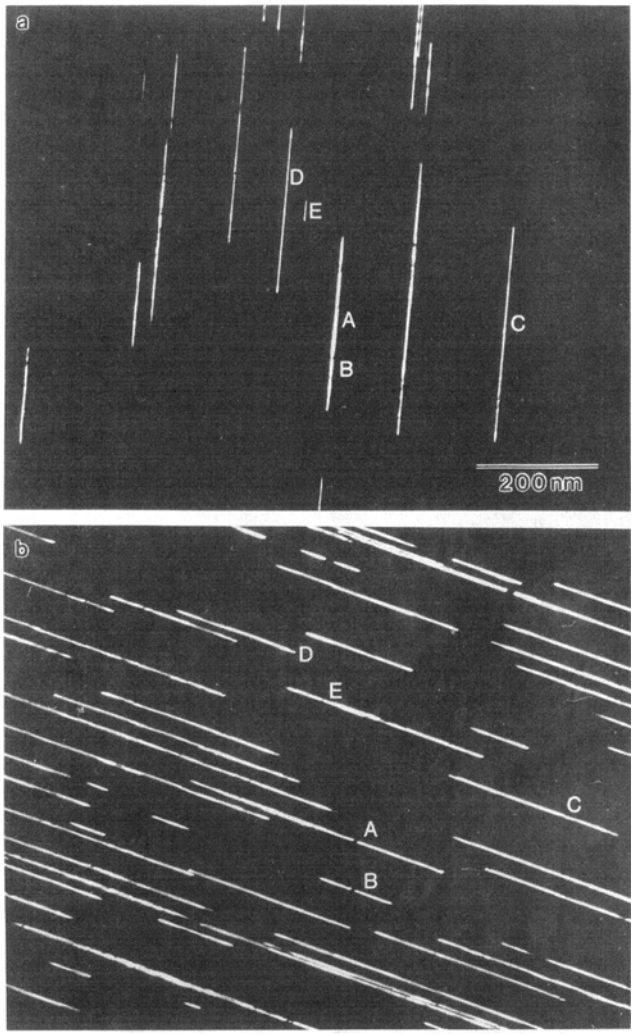

Fig. 2—T_1 centered DF TEM images for the variants on (*a*) $(11\bar{1})$ ($\mathbf{g} = 1/2[1\bar{1}1]$) and (*b*) $(\bar{1}11)$ ($\mathbf{g} = (1/2[\bar{1}11])$.

shape-factor effect of the thin T_1 plates has produced the intensity streaking observed along $(\bar{1}11)$ and $(1\bar{1}1)$.

The dark-field (DF) images shown in Figures 2(a) and (b) were constructed by tilting the crystal from the $\mathbf{B} = [110]$ orientation to more suitable two-beam conditions ($\mathbf{g} = [\bar{1}11]$ and $[1\bar{1}1]$, respectively) and using the $1/2(111)$ diffraction intensities. These coincide with T_1 (0002) spots. Inspection of the intersection points A, B, and C reveal that in cases where two T_1 variants completely penetrate one another, one of the variants displays a break in contrast at the intersection point. This finding suggests that the unbroken plate was present first and grew in such a way as to produce the intersection. The intersection in the region marked D shows where one plate variant has impinged upon a second plate variant during its growth. Finally, the intersection marked E appears to be the result of the formation of a new plate which has nucleated upon the broad face of a T_1 plate on the adjacent habit plane. These types of intersections are commonly observed between plates of any variant combination.

The region shown in Figures 1 and 2 may be tilted to the matrix zone orientation $\mathbf{B} = [013]$ to examine the broad faces of the plate variants $(\bar{1}11)$ and $(1\bar{1}1)$ (Figure 3).

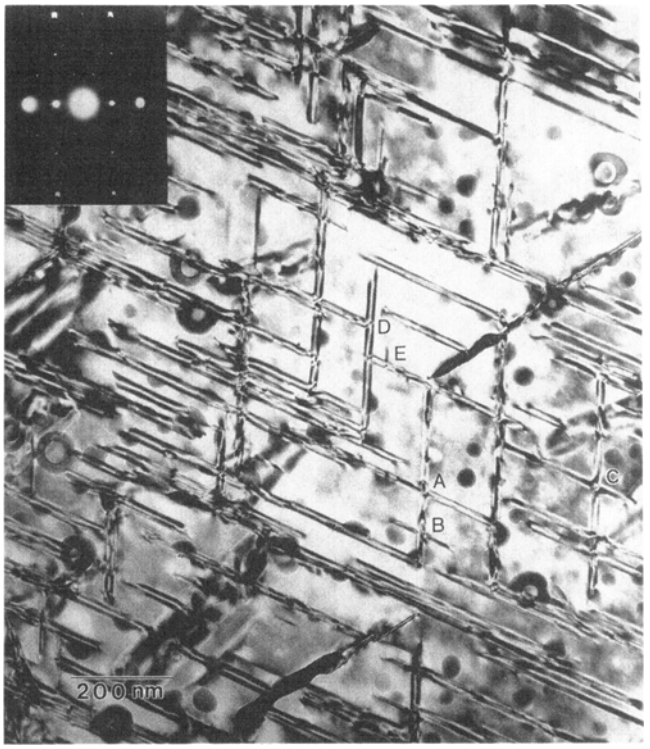

Fig. 3—BF image near $\mathbf{B} = [013]_{Al}$ at the same region shown in Fig. 1. Note that the T_1 plates parallel to $\mathbf{B} = [110]_{Al}$ are now equally inclined to **B**. Inset: SAD pattern for matrix orientation $\mathbf{B} = [013]$.

Similarly, DF images of the precipitate plates may be obtained by imaging T_1 diffraction intensity located at $1/3(131)_{Al}$-type positions. These are shown for $\mathbf{g} = 1/3(1\bar{3}1)$ and $1/3(\bar{1}\bar{3}1)$ in Figures 4(a) and (b), respectively. Several of the plates in the figures show regions of enhanced DF contrast due to additional thickness, which increases the diffracting volume of the plate. These layers have been added by growth ledges,[22] which are shown in the micrograph as the irregularly shaped boundaries between regions of contrast across the faces of the plates. The opposite ends of the newly added layers are usually very straight if they are initiated at a plate intersection or grew into another plate. Plate intersections have been previously suggested as nucleation sites,[23] and this possibility will be discussed later.

B. *The Interfacial Structure of T_1 Plate Faces*

To obtain strain contrast images of the interfacial structure on T_1 plates, it is necessary to use samples containing a low volume fraction and number density of plates. This is done to minimize plate overlap, which can mask or be confused with growth ledges, and to prevent the T_1/matrix interface from acquiring too many interfacial (intruder) dislocations from the matrix. To avoid these problems, the following studies were performed on unstretched material aged for relatively short periods of time. This section presents strain contrast results from experiments performed on material aged 1.5 hours to study plates one unit cell in thickness (Section 1) and 6 hours to examine multiple unit cell thick plates (Section 2) at 463 K (190 °C).

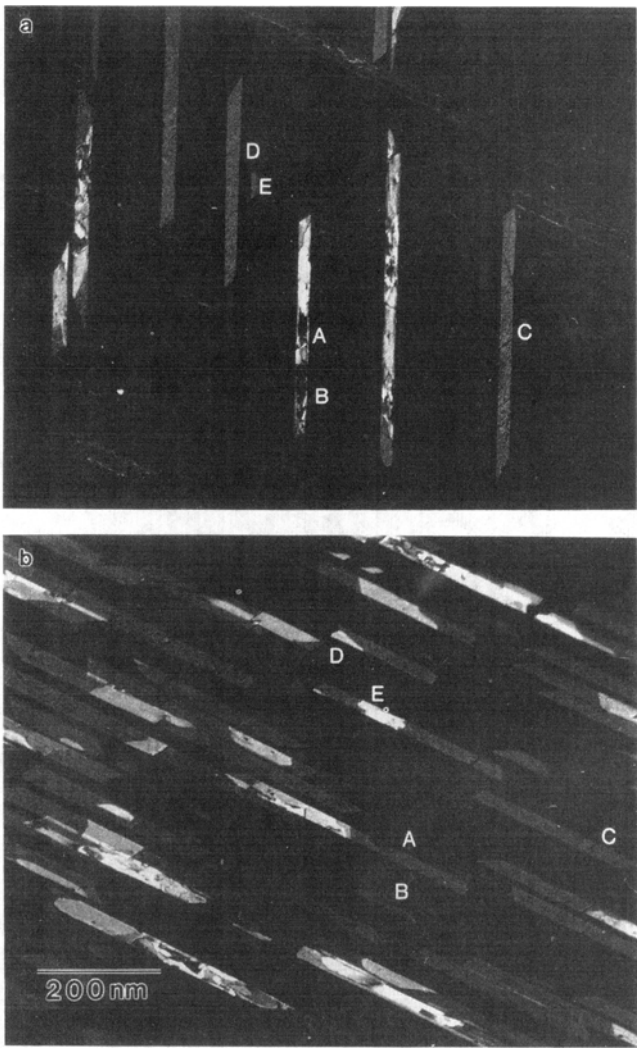

Fig. 4—DF images of T_1 plates near $\mathbf{B} = [103]_{Al}$ using (*a*) $\mathbf{g} = 2/3[1\bar{3}1]$ and (*b*) $\mathbf{g} = 2/3[\bar{1}\bar{3}1]$. Inset: SAD pattern at $\mathbf{B} = [112]_{Al}$ revealing T_1 diffraction intensity at 1/3{131}-type positions.

1. *Single growth ledge*

It was noted earlier that several T_1 plates may form intersections as the result of two variants growing into one another. This can also be observed at very early aging times (90 minutes/190 °C), and an example of such an intersection is shown in Figure 5. In this figure, the broad face of one plate variant, lying entirely in the foil, is oriented almost perpendicular to the beam axis ($\mathbf{B} \cong [111]$) in the two-beam condition $\mathbf{g} = [\bar{2}02]$. The habit plane of this plate is the (111) plane which is only about 5 deg from the plane of the micrograph. A second plate is seen as a dark band lying on the long axis of the first plate. Trace analysis indicates that this second plate is the variant on $(11\bar{1})$, which is tilted 10 to 12 deg from that position.

In the image condition $\mathbf{g} = [\bar{2}02]$, the variant on the (111) plane displays strong strain contrast around its perimeter. This is evident in the bright-field (BF) and DF images (Figures 5(a) and (b), respectively). The broad face of the plate does not show any other interfacial features. The **g**,3**g** weak-beam image where $\mathbf{g} = [\bar{2}02]$ (Figure 5(c)) also fails to reveal any additional features

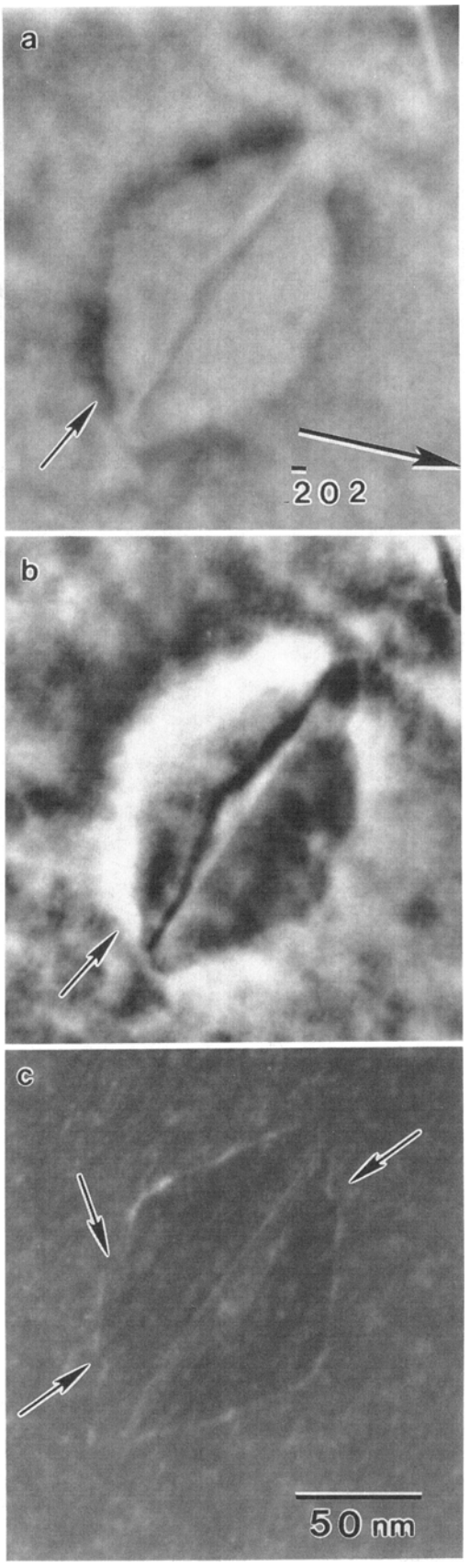

Fig. 5—Strain contrast images of T_1 plate on (111) in material aged 90 min at 190 °C showing dislocation contrast edges (*a*) $\mathbf{g} = [\bar{2}02]$, (*b*) $\mathbf{g} = [20\bar{2}]$, and (*c*) **g**,3**g**, $\mathbf{g} = [20\bar{2}]$ weak-beam image of dislocation at plate edges. Note kinks in dislocation line (arrows). See Table I for analysis.

other than the intersecting plate on $(11\bar{1})$. However, the fine details of the dislocation strain field seen at the edge of the plate in the BF and DF images are apparent. Several kinks (arrowed, Figure 5(c)), which have previously been shown to be important as atom addition sites during the growth of plate-shaped precipitates,[4,6] are visible along the dislocation.

The results of selected imaging conditions obtained by tilting this pair of plates are given in Table I. Examination of the plate on (111) in the different imaging conditions again failed to reveal any additional interfacial features. This finding suggests that the plate has resulted from the propagation of the indicated dislocations. New ledges, which would cause the plate to thicken, have not yet formed. Therefore, the plate variant on (111) can be considered as a new plate in its initial stage of growth, where the arrowed ledge is simply the edge of the plate. Imaging the plate under different conditions also reveals that the matrix displacement surrounding the plate can be described by two partial dislocations with nodes at either end of the second plate on $(11\bar{1})$. The possibility exists that the two plates may have nucleated cooperatively to form the observed intersection.

Analysis of the image contrast at the edge of the plate under various imaging conditions allows the character of the dislocations to be determined using the $\mathbf{g} \cdot \mathbf{b}$ criterion to construct a table of values for all of the possible Burgers vectors which might lie in the (111) matrix plane. The results of this analysis for the dislocations surrounding the plate shown in Figure 5 are also listed in Table I. Images produced for conditions of the type $\mathbf{g} = \langle 220 \rangle$ indicate that at least one extinction exists for each of the dislocations. From the table of $\mathbf{g} \cdot \mathbf{b}$ values, the presence of perfect dislocations with $1/2\langle 110 \rangle$-type Burgers vectors can be immediately eliminated, since these dislocations would be visible for all values of $\mathbf{g} = \langle 220 \rangle$. The Burgers vectors for the dislocations at the upper and lower halves of the plate edge can be deduced as partials $1/6[\bar{1}\bar{1}2]$ and $1/6[\bar{2}11]$, respectively. This analysis supports the proposed mechanism for the nucleation and growth of T_1 by the dissociation of matrix dislocations and propagation of partials by Noble and Thompson.[9] Given that the plate has nucleated at a perfect $\langle 110 \rangle$-type dislocation, the Burgers vector of the parent dislocation can be calculated from the partials as $1/2[\bar{1}01]$.

2. *Multiple growth layers*

The determination of the dislocation character of the first growth layer is the simplest case which can be considered for the T_1 growth interface. When the plates become thicker, several complications arise which make the analysis more difficult. These include the problems of intruder dislocations and plate overlap which were previously mentioned. Additionally, overlapping strain fields resulting from closely spaced partial dislocations on multiple layer growth ledges tend to confuse analysis of the ledges.[4]

Table I. Strain Contrast Analysis for T_1 Plate on (111)

	Observed	
g	Upper Side	Lower Side
$\bar{2}20$	—	visible
$\bar{2}02$	visible	visible
$0\bar{2}2$	visible	—
$11\bar{1}$	visible	—
$\bar{1}11$	—	visible
$1\bar{1}1$	—	—
200	—	visible
020	—	—

In order to produce four layers of hexagonal material from the fcc matrix, two partials must exist on the edge of a single growth ledge. The alignment of partials at the plate edges in thick plates is even more extensive since the plate edge includes several aligned ledges.[4,6] The following example has been chosen to illustrate and explain the effects of aligned partials on strain contrast.

The T_1 plates shown in Figures 6(a) through (g) (note that all micrographs are of the same area, *i.e.*, the same T_1 plates) ($\mathbf{B} \simeq 101$) are inclined with respect to the beam axis such that their interfacial structure can be examined. These plates were determined to be the variant on (111) by tilting the foil to various orientations. The sample containing the plates has been aged for 6 hours at 190 °C, and it is clear that the interfacial characteristics of these plates are more complicated than those seen after 90 minutes of aging (Figure 5). The T_1 plates in the figure have the appearance of laths because of truncation of the plate edges by the foil surfaces. Two other plate variants which are oriented on edge are seen in the micrograph. Several features of the plate variant on (111) have been lettered for further discussion.

The first feature considered is the plate ends or edges which lie inside of the foil. These are marked for two different plates at the points AA′ and EE′. The plate edges are faceted, with the facets determined by trace analysis to be in the direction of close packing in the (111) plane (*i.e.*, $\langle 110 \rangle$). If the strain contrast of the plate edges is studied under varying imaging conditions, the extinction conditions expected for $1/6\langle 112 \rangle$-type Burgers vectors are not always observed. The results of tilting to various conditions of $\mathbf{g}$ are listed in Table II for several of the features marked in the micrographs (Figures 6(a) through (g)).

Images of the plate edges at AA′ and EE′ produced for the three $\mathbf{g} = \langle 111 \rangle$-type reflections indicate that some weak contrast exists. Similarly, weak strain contrast exists for the plate ends in the condition where $\mathbf{g} = \langle 220 \rangle$. These observations are not limited to the plate ends, as the growth ledge at AC exhibits exactly the same behavior. The results suggest that the Burgers vectors of the dislocations at these points are mixed or have the image characteristics of both perfect ($\mathbf{b} = 1/2\langle 110 \rangle$) and partial ($\mathbf{b} = 1/6\langle 112 \rangle$) dislocations.

Similar behavior has been reported in the fcc → hcp transformation, producing γ' plates in the dilute Al-Ag system where nucleation and growth of the plate proceeds by an identical mechanism.[3,4] The growth ledges in γ' are two, or multiples of two, layers in height and bound by partials which are approximately aligned on every two layers.[6] The plate edges are comprised of one to several growth ledges which are approximately aligned, again with partials on every two layers. As the plates thicken by the passage of growth ledges, it is observed that the Burgers vectors of the partials tend to become increasingly mixed arrangements of the three types

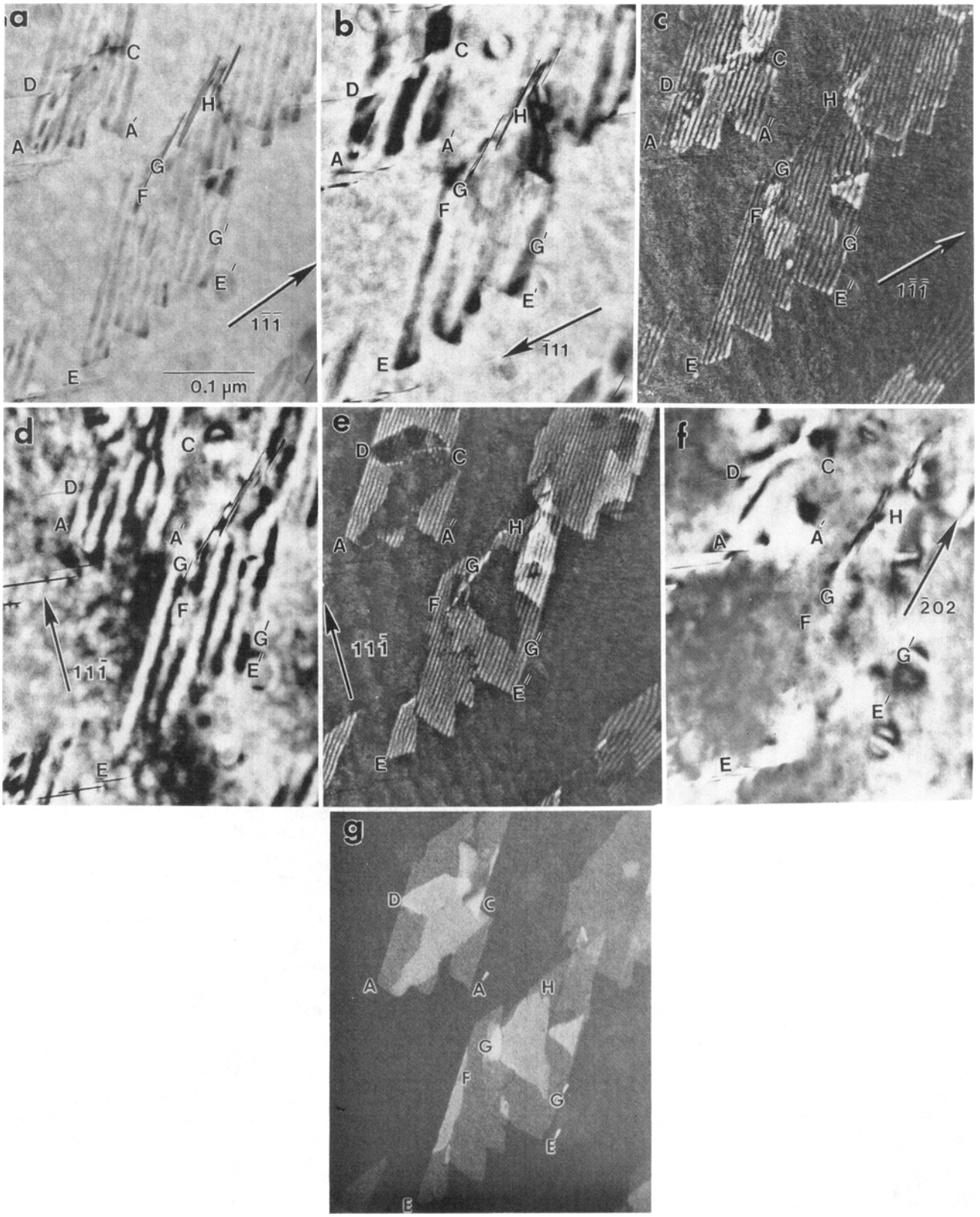

Fig. 6—Strain contrast images of T_1 plates on (111) in material aged for 6 h at 190 °C showing dislocation and stacking fault contrast: (*a*) **g** = [1$\bar{1}\bar{1}$], (*b*) **g** = [$\bar{1}$11], (*c*) **g**,3**g** weak-beam image, (*d*) **g** = [11$\bar{1}$], (*e*) **g**,3**g** weak-beam image, **g** = [11$\bar{1}$], (*f*) DF image, **g** = [$\bar{2}$02] (note extinction of stacking fault contrast), and (*g*) T_1 centered DF image, **g** = [20$\bar{2}$0].

Table II. Strain Contrast Analysis for T_1 Plates on (111)

Feature (Type)	g → $\bar{1}11$	$11\bar{1}$	$1\bar{1}1$	020	$\bar{2}02$	Comments
AA′ (edge)	weak	—	weak	weak	weak	like $1/2[1\bar{1}0]$ or $1/6[2\bar{1}\bar{1}] + 1/6[1\bar{2}1]$
BB′ (edge)	visible	—	—	weak	visible	like $1/2[1\bar{1}0]$ or $1/6[2\bar{1}\bar{1}] + 1/6[1\bar{2}1]$
AC (ledge)	visible	—	weak	visible	visible	like $1/2[1\bar{1}0]$ or $1/6[2\bar{1}\bar{1}] + 1/6[1\bar{2}1]$
DC (intruder)	—	visible	visible	—	visible	like $1/2[0\bar{1}1]$
EE′ (ledge)	weak	—	weak	weak	weak	like $1/2[1\bar{1}0]$ or $1/6[2\bar{1}\bar{1}] + 1/6[1\bar{2}1]$
FE′ (ledge)	weak	—	weak	weak	—	like $1/2[1\bar{1}0]$ or $1/6[2\bar{1}\bar{1}] + 1/6[1\bar{2}1]$
GG′ (ledge)	—	—	weak	weak	—	like $1/6[\bar{1}2\bar{1}]$
GH (intersection)	X	X	X	X	X	plate intersection
G′H (ledge)	—	visible	weak	weak	visible	like $1/6[11\bar{2}]$

$1/6\langle 112\rangle$ which can exist on the habit plane of the plate. The explanation for this[6,7] is based on the transformation tending toward producing the lowest volume strain as the plate thickens.

Therefore, the CTEM images of plate ledges and edges take on the characteristics of perfect dislocations as the plate thickens and greater alignment of partials occurs. However, the displacement will not be as localized as that of an equivalent but perfect dislocation. Therefore, the image is not expected to be as sharp. The growth ledge between the points AC and the plate edges at AA′ and EE′ provide good examples of this type of contrast mechanism. The strain contrast observed in each is indicative of a perfect Burgers vector, $\mathbf{b} = 1/2\langle 110\rangle$.

The micrographs in Figures 6(a) through (g) also provide an example of a growth ledge resulting from the alignment of two partials which have the same displacement. This is seen between the marked points GG′H, which is a triangular-shaped area bordered at GH by an intersecting plate on a different variant (most clearly seen in Figure 6(g)). In this case, the contrast analysis in Table II reveals that the dislocations between GG′ and HG′ are of the types $1/6[\bar{1}2\bar{1}]$ and $1/6[11\bar{2}]$, respectively. These partials are joined at a node at point G′ and have presumably resulted from dissociation of the perfect dislocation $1/2[01\bar{1}]$. Assuming that the ledge created by dissociation is four layers high, then two partials of the same type would be aligned at the ledge edge (*i.e.*, GG′ and HG′) normal to the plate face. In this case, the net effect of the resulting displacements would be $[11\bar{2}]$ and $[\bar{1}2\bar{1}]$ types for GG′ and HG′, respectively. The magnitude of the displacement is changed, but the direction remains constant. The resulting image can, therefore, be expected to exhibit the contrast of its component partials when **g** is of the type $\langle 220\rangle$. However, when **g** is of the $\langle 111\rangle$ type, the magnitude of the dot products of $\mathbf{g}\cdot\mathbf{b}$ has increased, and therefore, weak contrast is observed for the imaging conditions where extinction is normally expected. This is generally found to be the case for the images of ledges of this type observed in the present study (Table II). As in the previous case of aligned partials of different Burgers vectors, the intensity of the observed strain contrast is limited by overlapping strain fields. The alignment of partials in different layers at the edge of the ledge will cause the strain to be less localized and broaden the image width.

The displacement fringe contrast observed in the images shown in Figures 6(a) through (e) is indicative of the fact that the precipitate plate has formed by the movement of partial dislocations $1/6\langle 112\rangle$ at the growth interface. Additionally, the net displacement between the close-packed aluminum layers above and below the precipitate plate is altered by the displacement added by the passage of each successive growth ledge. This is illustrated by the shifts in fringe contrast associated with growth ledges in the **g**,3**g** DF images (Figures 6(c) and (e)). The visibility of fringes produced by displacement of the type $1/6\langle 112\rangle$ is determined by the change in phase between the aluminum close-packed planes above and below the precipitate. For any imaging condition, **g**, a phase factor α may be defined using the relationship[24]

$$\alpha = \frac{2\pi[\mathbf{g}\cdot\mathbf{R}]}{6}$$

where **R** is the total displacement created by the passage of partials. Displacement fringes are visible for any imaging condition such that the value of $\alpha = \mp 2\pi/3$. This is true for $\mathbf{g} = [\bar{1}11]$ (Figures 6(a) through (c)) and $\mathbf{g} = [11\bar{1}]$ (Figures 6(d) and (e)). The fault is not observed in Figure 6(f), because $\mathbf{g} = [202]$ and α has a value of zero.

Similarly, the extinction of fringe contrast in certain regions of Figure 6(e) is due to the changes in phase introduced by the passage of growth ledges. In the region HGG′, the additional plate thickness produced by the passage of partials comprising a growth ledge has produced a change in α that, for this imaging condition **g**,

is very close to zero. However, fringe contrast is observed in the same region when $\mathbf{g} = [111]$ (Figure 6(c)), as α has a nonzero value for this imaging condition.

Growth ledges on the precipitate plates can also be seen in the T_1 centered DF images (Figure 6(g)) where $\mathbf{g} = [20\bar{2}0]_{T_1}$. Regions of increased plate thickness are associated with an increase in contrast because of the larger diffraction volume. The ledge constituting the region HGG′ can be seen very clearly in this micrograph. The height of a growth ledge revealed with HREM (Figure 7) is four layers and is the minimum height observed in our studies.

C. *Nucleation and Growth of T_1 Plates*

In this section, the general observations of T_1 plate growth, both edgewise and thickening, using high-resolution microscopy will be presented. Based on these observations and those of CTEM, a mechanism for growth and nucleation of T_1 plates is proposed.

1. *General observations*

The high-resolution micrographs in Figure 8 illustrate the important features of T_1 plates in material which has been stretched 6 pct and aged 3 hours at (463 K) 190 °C. During this aging interval, the T_1 plate distribution is in a state of rapid evolution. The volume fraction of T_1, the number density of plates, and the average plate thickness are all increasing (see companion paper.[26])

In Figure 8(a), the intersection of two plate variants is shown in the orientation $\mathbf{B} = [101]$. At the point marked A, a new growth layer is evident with two growth ledges at its ends. It is obvious that the propagation of these ledges in opposite directions will result in increasing the thickness of the plate by four layers or one T_1 cell. A pair of growth ledges in this configuration is expected from the dissociation of an intruder dislocation with a Burgers vector in the plane of the plate (*i.e.*, $\mathbf{b} = 1/2[110]$ type). The origin of the growth ledge indicated at the points B, C, D, and E, however, is not so apparent.

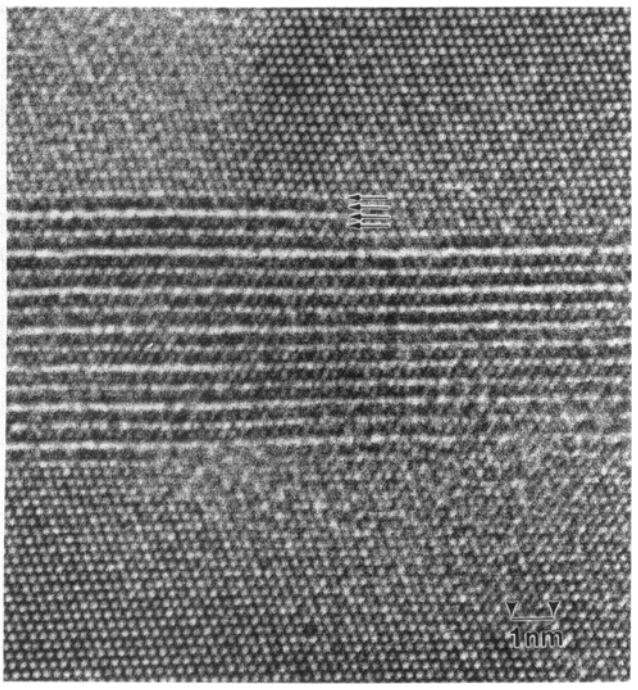

Fig. 7—High-resolution image of T_1 plate showing growth ledge. $\mathbf{B} = [110]_{Al}$ aged 550 h at 190 °C.

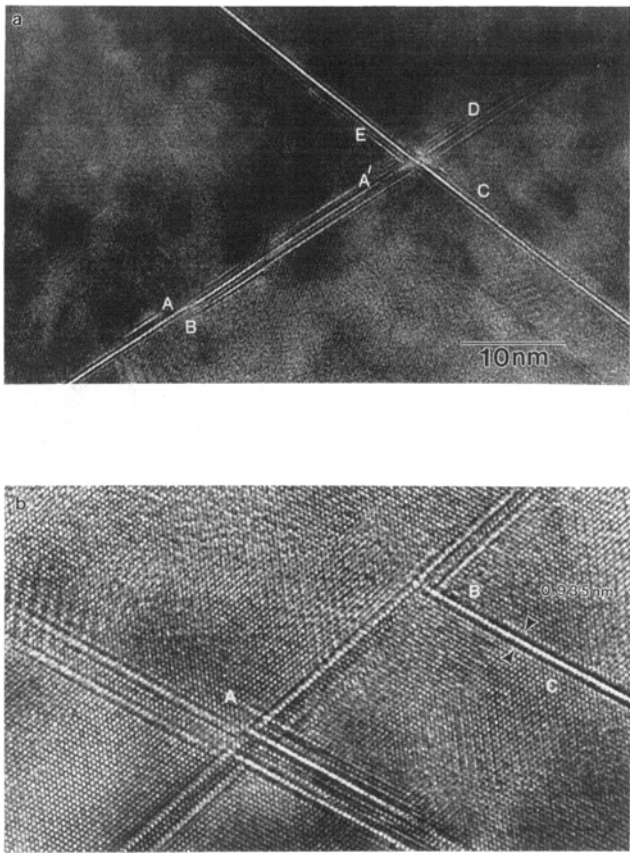

Fig. 8—High-resolution images of T_1 plates in material aged 3 h at 190 °C: (*a*) $\mathbf{B} = [110]_{Al}$ or $\mathbf{B} = [01\bar{1}0]_{T_1}$ and (*b*) same orientation as (a) but a different region.

In the latter cases, the four new layers associated with the growth ledges terminate at the intersection of their host plate and a second T_1 variant. It is not clear that these layers grew into the intersecting variant or if the single growth ledges producing the new layers nucleated at the intersection of the two plates. The fact that a growth ledge can terminate at such an intersection is clear, and this would most likely be the fate of the ledge at point A′ with further propagation.

Plate intersections have been reported to be nucleation sources for new growth ledges[23] in similar systems, and such a mechanism could be important for T_1 plates as well. Evidence for such nucleation is seen at the point marked A in Figure 8(b), where a new ledge has apparently formed at the intersection of two variants of T_1 plates. The point marked B in Figure 8(b) shows two impinging plates. This intersection could conceivably result from a number of sources; for example, the plate marked C could have simply grown into the second variant, or perhaps the plate was nucleated at a defect (*e.g.*, an intruder dislocation or growth ledge) on the broad face of the second variant. The latter explanation would also explain the additional thickness observed on the side of the second variant above the intersection point (upper

right of Figure 8(b)). In any event, the plate marked C is the thinnest T_1 plate observed. This plate is four planes in thickness, because nucleation of a four-layer plate yields a thickness equal to one T_1 unit cell (this assumes that we count 1/2 each of the outer, almost pure Al planes as part of the T_1 unit cell). The outermost layer of T_1 plates is an Al-rich chemical layer, as originally proposed by Huang and Ardell[15] and supported by Howe *et al.*,[20] which is most easily seen in the beam direction $\mathbf{B} = [1\bar{2}10]$ (Figure 9). The outer Al-rich layer at the T_1/matrix interface is not as obvious when the beam direction is [0110] (Figure 7), because the matrix planes yield similar contrast and spacing in this orientation ($\mathbf{B} = [110]$) and the outer layer blends with the matrix. This causes the plate marked C in Figure 8(b) to only appear three layers in thickness. This result agrees with published micrographs by Radmilovich and Thomas[21] and Howe *et al.*[20]

2. *A mechanism for nucleation and growth of T_1 plates*

The experimental observations of this study allow a number of conclusions concerning the nucleation and growth of T_1 plates to be made. Any attempt to propose a nucleation and growth mechanism for T_1 plates must be able to account for the following features:

(1) The critical plate thickness for T_1 nucleation is four 0001 layers since this thickness corresponds to exactly one unit cell.
(2) The interfacial chemical layer is always an Al-rich layer in the proposed structure.[15,20]
(3) Growth ledges on T_1 plates add four new layers or one unit cell to the plate thickness. The chemical stacking sequence of the growth ledge is such that the outer Al-rich layer is maintained at the T_1/matrix interface.
(4) Compositional faults are produced by five layer growth ledges which add the layers to an existing plate. The total thickness of plates with a compositional fault is no longer an integral number of T_1 cells.

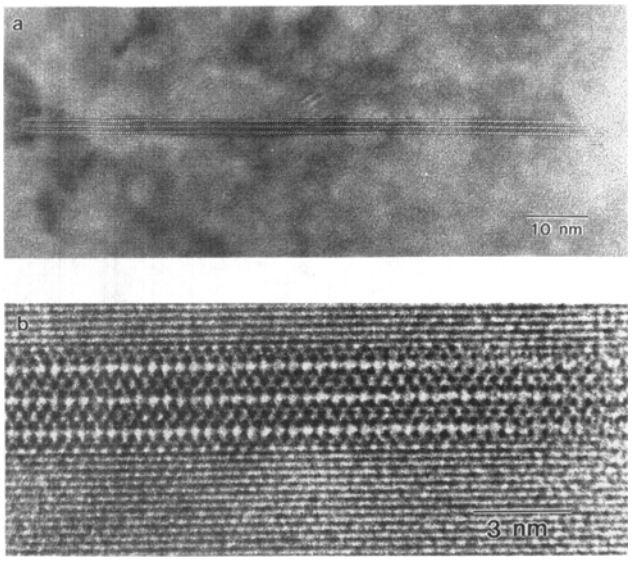

Fig. 9—(*a*) High-resolution image of T_1 plate where $\mathbf{B} = [\bar{1}\bar{1}2]_{Al}$ or $\mathbf{B} = [1210]_{T_1}$. (*b*) Enlargement of (a) near edge showing stacking of $(0001)_{T_1}$ planes.

(5) The plates and plate ledges are always bounded by partial dislocations ($1/6\langle 112\rangle$). The nucleation and growth of T_1 plates are governed by the movement of these partial dislocations which transform the fcc stacking in the matrix into the hexagonal stacking required for the T_1 structure.

To form a T_1 unit cell of four perfectly stacked (2 half-layers of Al on the outside of the plate) hexagonal (0001) layers in a fcc matrix, two partial dislocations are necessary for each growth ledge. The two partial dislocations can be considered to originate from a number of different sources. The most likely are dislocation jogs and cross-slipped screw segments of perfect matrix dislocations, because the density of these types of defects is increased during stretching prior to aging. An increase in the number of such defects also explains the large increase in T_1 number density observed with stretching.[1]

The following model of T_1 plate nucleation is suggested to illustrate the role of a dislocation jog. Consider the case of an idealized jog two (111) planes high separating two edge dislocation segments whose Burgers vector lies in (111) (Figure 10). The atomic mechanism of the Huang and Ardell model[15] was shown to be feasible by the glide of partial dislocations on alternate (111) planes,[1] whereas the Howe *et al.*[20] model requires the two dislocations on neighboring planes. Such a jog may be created by the passage of an edge dislocation on (111) or adjacent glide planes, with a Burgers vector which is perpendicular to the Burgers vector of the dislocation on (111). The jog could also be created by climb. In either

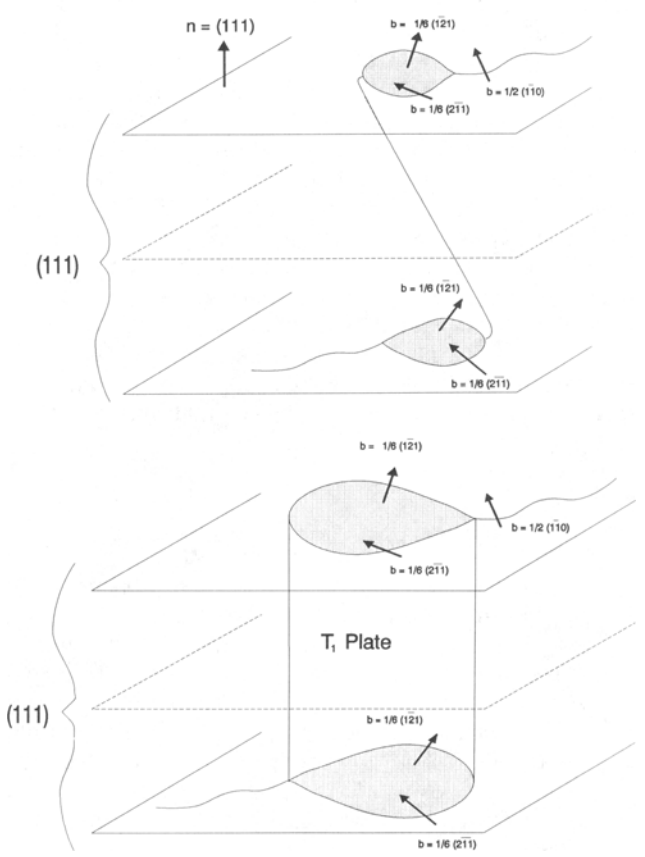

Fig. 10—Schematic diagram of mechanism for T_1 plate nucleation on dislocation jog.

event, dissociation of the dislocation segments at the nodes created by the jog on the different (111) layers will result in the displacements required for T_1 nucleation. A cross-slipped screw segment separating the dislocation on alternate (111) layers will also produce a similar arrangement of partials, giving the desired displacement.

The formation and growth of the T_1 plate by this mechanism proceeds by the coordinated movement of the partials on each plane. The strain contrast experiments previously discussed suggest that the partials on alternate planes couple to form the growth ledge. In the newly formed plate, the partials on either plane are identical, and coupling of partials can occur in one or two possible ways. The growth ledges can exist as two coupled $1/6[2\bar{1}\bar{1}]$ dislocations and two $1/6[1\bar{2}1]$ dislocations (shown in Figure 10(b)) or as mixed couples of $1/6[2\bar{1}\bar{1}]$ and $1/6[1\bar{2}1]$ dislocations as growth ledges. The latter case will give the contrast of a perfect [110]-type dislocation.

The nucleation of a new growth ledge is a simple variation on the plate nucleation mechanism outlined above. An intruder dislocation with either a screw segment lying out of the interfacial plane or a jog in an edge dislocation can similarly dissociate on two adjacent (111) layers. This yields the necessary displacement for a ledge which adds four new T_1 layers to the thickness of the T_1 plate. Again, coupling of the two partials to form the ledges may favor mixed partial Burgers vectors. Either will produce a perfectly sequenced plate (*i.e.*, free of stacking defects).

The model for T_1 nucleation and growth is consistent with all of the experimental findings of this study and others (1,15,20) and is useful for predicting the stacking sequences for T_1 plates of any thickness, as well as including stacking defects. The current results do, however, argue against the traditionally held view of "stacking fault" nucleation of plates, *e.g.*, T_1 and γ'. This is supported by the observation that T_1 nucleation is not enhanced by natural aging prior to artificial aging and is enhanced by plastic deformation.[25] The current experimental evidence shows that the initial plate thickness is four layers, requiring a minimum passage of two partial dislocations. A single stacking fault cannot produce this displacement without closing and cross slipping (*via* a jog). Therefore, it seems that such an exotic mechanism need not be invoked. Clearly, this is an area that needs to be re-examined with current high-resolution techniques.

IV. SUMMARY OF RESULTS

1. The nucleation and growth of T_1 plates occur by the mechanism of dissociation of matrix dislocations into partials ($1/6\langle 112\rangle$) which form the growth interface of the plate and the plate edges.
2. Strain contrast analysis of T_1 plate images produced similar results to those reported for γ' plates in dilute Al-Ag alloys.[4,5] Movement of the plate edges and the edges of growth ledges, which consist of stacked partial dislocations, results from the propagation of ledge kinks.
3. Strain contrast analysis of the Burgers vector of plate edges and the edges of growth ledges indicates the stacking of partials of mixed displacement. This is presumably due to the beneficial lowering of the volume strain produced by the transformation by such arrangements.
4. Analysis of structure images reveals that the initial nucleation of T_1 plates produces a four (0001)-layer hexagonal plate (one unit cell), and subsequent plate thickening is accomplished by growth ledges which add four new layers of T_1 material on their passage across the broad face of the plate.
5. New ledges are nucleated at intruder dislocations which have Burgers vectors in the plane of the T_1/matrix interface. Evidence also exists for ledge or plate nucleation at the intersections of two variants; however, further study is needed to verify this possibility.
6. T_1 plate nucleation can be modeled on the dissociation of a dislocation on opposite sides of a jog (or cross-slipped screw segment) one or two (111) planes high. Such dissociation will account for all of the observed T_1 plate characteristics. The transformation produces a four-layer hexagonal plate by the coupling of partials on these layers, and the model can produce either perfect or imperfect stacking with displacement faults.
7. The nucleation of growth ledges on existing plates can also be modeled by the same mechanism. An intruder dislocation ($\mathbf{b} = 1/2\langle 110\rangle$ in the interfacial plane) with a one or two (111) matrix layer high jog out of the interfacial plane can dissociate into partials on the alternate layers. The partials on these layers can then couple to form the ledge.
8. The influence of stretching will not only increase the number of dislocations but, more importantly, the number of dislocation jogs. The model of T_1 nucleation at jogs is, therefore, consistent with experimental observations derived from the plate distributions.

ACKNOWLEDGMENTS

This work was sponsored by the United States Army Research office under government Contract No. DAAL03-86-K0128, Dr. Andrew Crowson, Director. We gratefully acknowledge use of the Atomic Resolution Microscope at the National Center for Electron Microscopy, Lawrence Berkeley Laboratories, Berkeley, CA, and to Mr. Chris Nelson in particular for expert assistance.

REFERENCES

1. W.A. Cassada, G.J. Shiflet, and E.A. Starke, Jr.: *J. Phys.*, 1988, vol. 48, supp. C3 (9), pp. 397-406.
2. R.B. Nicholson and J. Nutting: *Acta Metall.*, 1961, vol. 9, p. 332.
3. J.A. Hren and F. Thomas: *Trans. TMS-AIME*, 1963, vol. 227, pp. 308-18.
4. J.M. Howe, H.I. Aaronson, and R. Gronsky: *Acta Metall.*, 1985, vol. 33, pp. 639-48.
5. J.M. Howe, H.I. Aaronson, and R. Gronsky: *Acta Metall.*, 1985, vol. 33, pp. 649-58.
6. J.M. Howe, U. Dahmen, and R. Gronsky: *Phil. Mag. A*, 1987, vol. 56 (1), pp. 31-63.
7. H.K. Hardy and J.M. Silcock: *J. Inst. Met.*, 1955–56, vol. 84, pp. 423-28.
8. J.M. Silcock: *J. Inst. Met.*, 1959–60, vol. 88, pp. 357-64.

9. B. Nobel and G.E. Thompson: *J. Met. Sci.*, 1972, vol. 6, pp. 167-74.
10. L.F. Mondolfo: *Aluminum Alloys—Structure and Properties*, Butterworth's, London, 1979, p. 577.
11. S. Kerry and V.D. Scott: *Met. Sci.*, 1984, vol. 18, pp. 289-94.
12. V.D. Scott, S. Kerry, and R.L. Trumper: *Mater. Sci. Technol.*, 1987, vol. 3, pp. 827-35.
13. T.J. Langan and J.R. Pickens: *5th Int. Al-Li Conf.*, 1989, E.A. Starke and T.H. Sanders, eds., Materials and Component Eng. Pub., Birmingham, United Kingdom, pp. 691-700.
14. U. Dahmen and K. Westmacott: *Phys. Status Solidi A*, 1983, vol. 80, pp. 249-62.
15. J.C. Huang and A.J. Ardell: *Mater. Sci. Technol.*, 1987, vol. 3, pp. 176-88.
16. R.J. Rioja and E.A. Ludwiczak: in *Aluminum Lithium Alloys III*, The Institute of Metals, London, 1986, pp. 471-82.
17. A.K. Eikum and G.H. Narayanan: *Proc. 44th Annual Meeting of the Electron Society of America*, G.W. Bailey, ed., San Francisco Press, San Francisco, CA, 1986, pp. 550-51.
18. W.A. Cassada, G.J. Shiflet, and E.A. Starke, Jr.: *Scripta Metall.*, 1987, vol. 21, pp. 387-92.
19. K.S. Vecchio and D.B. Williams: *Metall. Trans. A*, 1988, vol. 19A, pp. 2885-91.
20. J.M. Howe, J. Lee, and A.K. Vasudevan: *Metall. Trans. A*, 1988, vol. 19A, pp. 2911-20.
21. V. Radmilovich and G. Thomas: *J. Phys.*, 1988, vol. 48, supp. C3 (9), pp. 385-96.
22. H.I. Aaronson: in *Decomposition of Austenite by Diffusional Processes*, V.F. Zackay and H.I. Aaronson, eds., Interscience, New York, NY, 1962, p. 387-548.
23. K.E. Rajab and R.D. Doherty: in *Int. Conf. on Solid-Solid Phase Transfer*, H.I. Aaronson, D.E. Laughlin, R.F. Sekerka, and C.M. Wayman, eds., TMS-AIME, Warrendale, PA, 1982, p. 555.
24. G. Thomas and M.V. Goringe: *Transmission Electron Microscopy of Materials*, John Wiley & Sons, New York, NY, 1979.
25. R.F. Ashton, D.S. Thompson, and G.W. Gayle: *Proc. Conf. on Aluminum Alloys*, E.A. Starke and T.H. Sanders, eds., Engineering Materials Adv. Services, Warley, United Kingdom, 1986, vol. I, pp. 403-17.
26. W.A. Cassada, G.J. Shiflet, and E.A. Starke, Jr.: *Metall. Trans. A*, 1991, vol. 22A, pp. 299-306.